CardioRenal Medicine

Cardiorenal Med 2012;2:66–82
DOI: 10.1159/000335565
Received: November 29, 2011
Accepted: December 5, 2011
Published online: January 27, 2012

1664–3828/12/0021–0066$38.00/0
www.karger.com/crm

Original Paper

Ultrastructure Study of Transgenic Ren2 Rat Aorta – Part 1: Endothelium and Intima

Melvin R. Hayden[a, b, e] Javad Habibi[a, b, e, f] Tejaswini Joginpally[e]
Poorna R. Karuparthi[a, c] James R. Sowers[a, b, d–f]

Departments of [a]Internal Medicine, [b]Endocrinology Diabetes and Metabolism, [c]Cardiovascular Disease and [d]Medical Physiology and Pharmacology, and [e]Diabetes and Cardiovascular Disease Center, University of Missouri-Columbia School of Medicine, and [f]Harry S. Truman VA Medical Center, Columbia, Mo., USA

Key Words
Angiotensin II · Extracellular matrix remodeling · Hypertension · Intima · NADPH oxidase · Oxidative stress · Type 2 diabetes mellitus

Abstract
Background: The renin-angiotensin-aldosterone system plays an important role in the development and progression of hypertension and accelerated atherosclerosis (atherosclerosis) associated with the cardiorenal metabolic syndrome and type 2 diabetes mellitus. Additionally, the renin-angiotensin-aldosterone system plays an important role in vascular-endothelial-intimal cellular and extracellular remodeling. ***Methods:*** Thoracic aortas of young male transgenic heterozygous (mRen2)27 (Ren2) rats were utilized for this ultrastructural study. This lean model of hypertension, insulin resistance and oxidative stress harbors the mouse renin gene with increased local tissue (aortic) levels of angiotensin II and angiotensin type 1 receptors and elevated plasma aldosterone levels. ***Results:*** The ultrastructural observations included marked endothelial cell retraction, separation, terminal nuclear lifting, adjacent duplication, apoptosis and a suggestion of endothelial progenitor cell attachment. The endothelium demonstrated increased caveolae, microparticles, depletion of Weibel-Palade bodies, loss of cell-cell and basal adhesion hemidesmosome-like structures, platelet adhesion and genesis of subendothelial neointima. ***Conclusion:*** These observational ultrastructural studies of the transgenic Ren2 vasculature provide an in-depth evaluation of early abnormal remodeling changes within conduit-elastic arteries under conditions of increased local levels of angiotensin II, oxidative stress, insulin resistance and hypertension.

Melvin R. Hayden, MD

Department of Internal Medicine
University of Missouri-Columbia School of Medicine
Health Sciences Center, MA410, DC043.00, Columbia, MO 65212 (USA)
Tel. +1 573 346 3019, E-Mail mrh29@usmo.com

CardioRenal Medicine

Cardiorenal Med 2012;2:66–82

DOI: 10.1159/000335565
Published online: January 27, 2012

www.karger.com/crm

Introduction

Accelerated atherosclerosis (atherosclerosis) occurs in the cardiorenal metabolic syndrome (CRS), which includes the constellation of hyperlipidemia, hyperinsulinemia, hypertension (HTN), dysglycemia, insulin resistance (IR), impaired renal function and oxidative stress (OS) [1–15] (fig. 1). CRS and type 2 diabetes mellitus (T2DM) result in a marked increase in cardiovascular disease (CVD) and renal disease morbidity and mortality. Therefore, we have chosen to study the early ultrastructural remodeling in aortas from young male transgenic rats in a model of HTN, IR, OS, proteinuria and impaired glucose tolerance (IGT) (fig. 2). These rats develop early CVD and IR manifested in the heart, kidney, pancreas, skeletal muscle and vasculature [1–15].

The male transgenic heterozygous (mRen2)27 (Ren2) rat overexpresses the mouse renin gene and is known to have increased local tissue levels of angiotensin II (Ang II), low plasma renin activity and increased plasma levels of aldosterone [1–15]. Transgenic Ren2 rats manifest an activated renin-angiotensin-aldosterone system (RAAS) and altered autonomic nervous system regulation [1–15].

Previous studies have demonstrated that the major cellular and extracellular remodeling and signaling mechanisms have been improved by RAAS blockade including direct renin inhibition [1–15] and amelioration of OS with the antioxidant tempol, a superoxide dismutase mimetic [1, 3, 5, 7, 11, 14]. Treatment with the third-generation β_1-adrenoceptor blocker nebivolol has been shown to decrease nicotinamide adenine diphosphate-reduced (NADPH) oxidase activity and increase the bioavailability of endothelial-derived nitric oxide, with resultant attenuation of renal ultrastructural remodeling and albuminuria in this model [16, 17].

The vasculature undergoes dynamic structural changes by a process termed vascular remodeling, which involves cell growth, migration, phenotypic changes and extracellular matrix synthesis and degradation. The layers of conduit-elastic arteries such as the thoracic aorta have been classically divided into three distinct layers: the tunica intima, the media and the adventitia. In healthy young mammals, endothelial cells (ECs) are found only in the intima, vascular smooth muscle cells (VSMCs) in the media and connective tissue cells in the adventitia [18, 19].

Because young (9–10-week-old) male Ren2 rats and their Sprague Dawley controls (SDC) have not developed a subendothelial space or intima, and ECs directly abut and adhere to the internal elastic lamina (IEL), we compare and discuss each of the following layers: endothelium, IEL, media, external elastic lamina and adventitia (fig. 2, 3) in this two-part series. We also discuss the unique observation of the genesis of a neointima in the young Ren2 rat model. Ultrastructural observations of these young Ren2 rat aortas increase our knowledge regarding some of the earliest changes that occur in HTN and the associated accelerated atherosclerosis (atherosclerosis) in the CRS and T2DM in human patients.

Animals and Methods

Animals and Treatments

Animal care and procedures were approved by and followed the University of Missouri Animal Care and Use Committee and NIH guidelines. Ren2 heterozygous (+/–) and SDC littermate rats were received at 5–6 weeks of age from Wake Forest University, Winston-Salem, N.C., USA. After arrival, the animals were allowed 1 week to become acclimatized to the environment, had free access to standard chow and tap water and were sacrificed at 9–10 weeks of age.

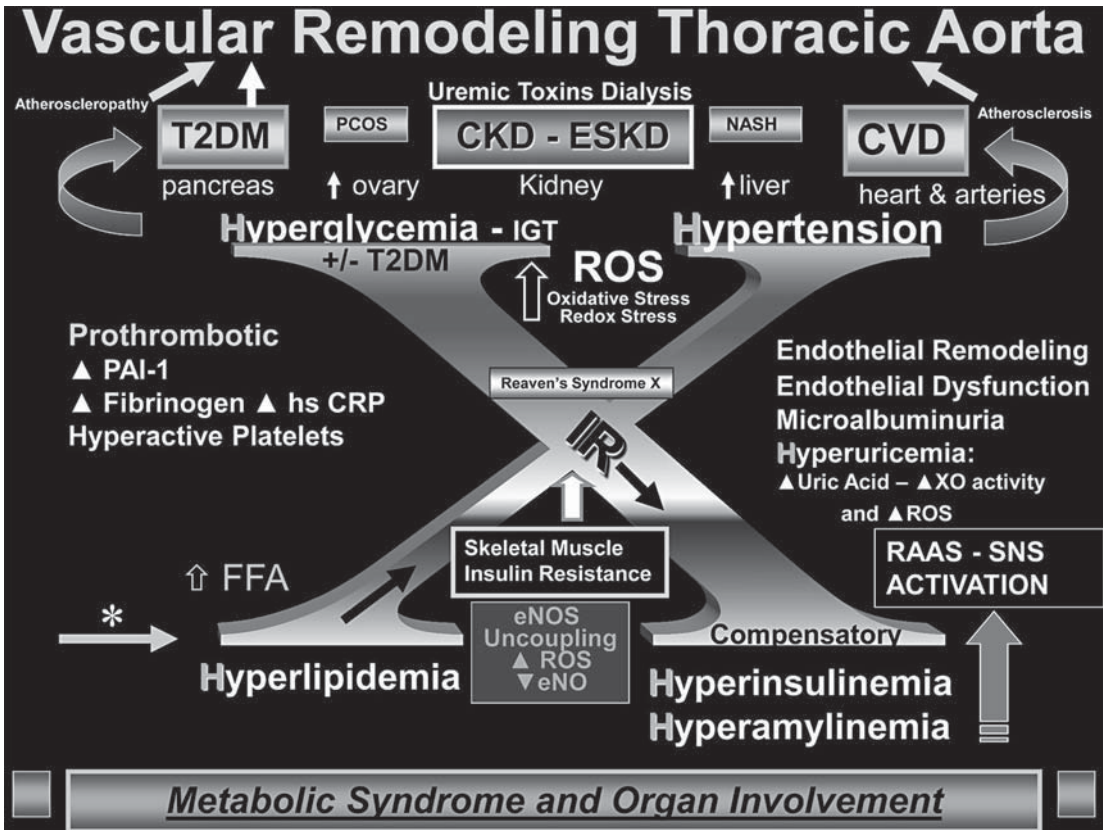

Fig. 1. Vascular remodeling of the thoracic aorta in the Ren2 rat. This image demonstrates the 'H' phenomenon consisting of hyperlipidemia, hyperinsulinemia and hyperamylinemia, hypertension and hyperglycemia (IGT) and how these may lead to the development of end-organ remodeling, including vascular remodeling of the thoracic aorta. This complex interplay of multiple metabolic toxicities is placed on a background of Reaven's now classic syndrome X. In obesity models and human obesity, the RAAS and the sympathetic nervous system (SNS) are activated partially in response to obesity, whereas in the transgenic Ren2 rat model the RAAS is genetically increased in the local tissue levels along with systemic activation and the SNS. PCOS = Polycystic ovarian syndrome; CKD = chronic kidney disease; ESKD = end-stage kidney disease; NASH = non-alcoholic steatohepatitis; PAI-1 = plasminogen activator inhibitor-1; hs CRP = highly sensitive C-reactive protein; XO = xanthine oxidase; FFA = free fatty acid; eNOS = endothelial nitric oxide synthase; eNO = endothelial-derived nitric oxide.

Systolic Blood Pressure, Weight and Blood Glucose

Restraint conditioning was initiated on the day of initial systolic blood pressure measurement which was measured in triplicate, on separate occasions throughout the day, using the tail-cuff method (Student Oscillometric Recorder; Harvard Systems Hatternas Instrument Inc., Cary, N.C., USA), and on the day prior to sacrifice. Following an overnight fast, blood was collected from the tail vein prior to sacrifice to determine baseline glucose. Glucose levels were determined on whole blood samples using a glucose oxidase method (OneTouch Ultra glucose analyzer; Lifescan, Inc., Milpitas, Calif., USA).

Transmission Electronic Microscopy

Descending thoracic aorta tissue was thinly sliced and placed in primary transmission electronic microscopy (TEM) fixative, followed by secondary fixation with acetone dehydration and Epon-Spurr's resin infiltration. Using Ultracut UCT with a diamond knife (Diatome, Biel, Switzerland), 85-nm-thin sections were prepared. The specimens were then stained with 5% uranyl acetate and Sato's triple-lead stain. A transmission electron microscope (JEM-1400 Electron Microscope) was utilized to view all samples.

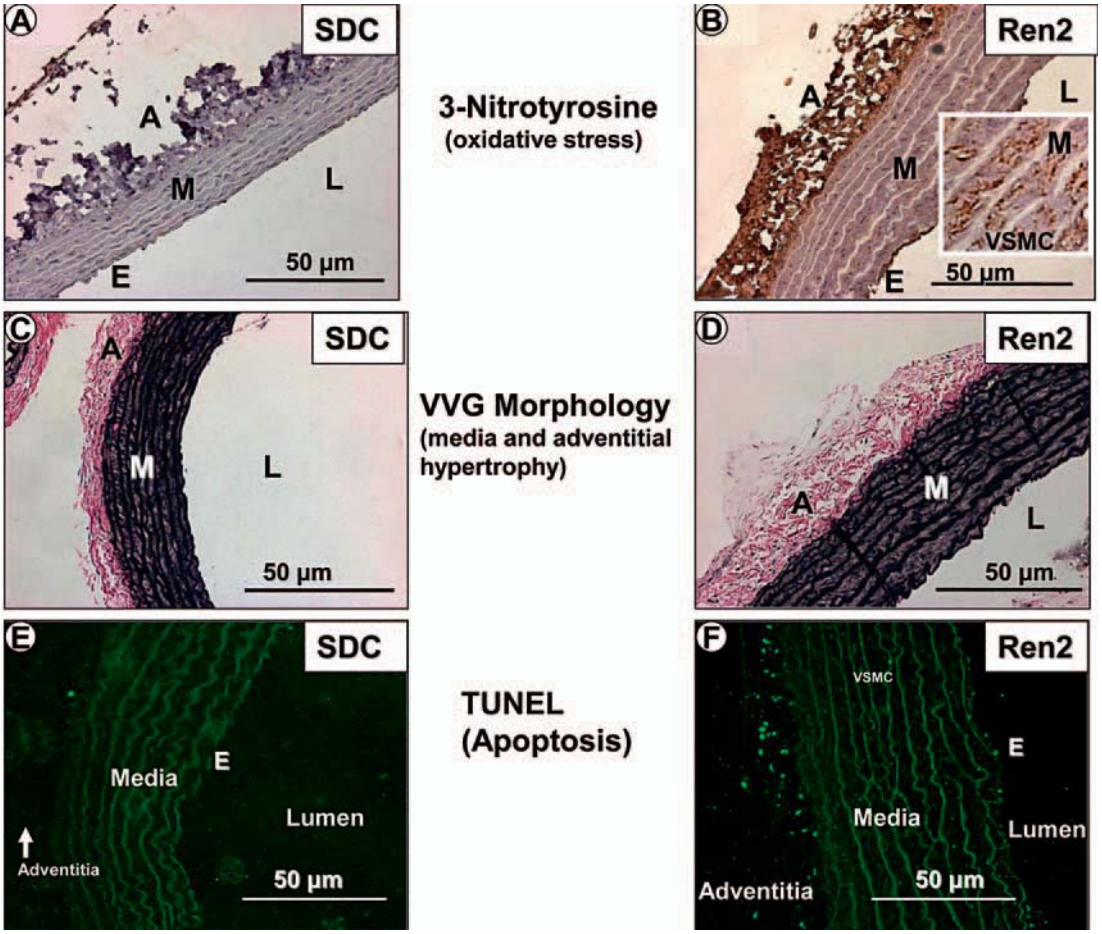

Fig. 2. OS, media and adventitial expansion as well as apoptosis in the Ren2 rat aorta. The three major layers of the thoracic aorta are represented by the endothelium (E), media (M) and adventitia (A). Representative images depict marked OS as demonstrated by increased 3-nitrotyrosine staining (rust color) in the Ren2 model (**B**) as compared to the SDC model (**A**) in all three layers of the aorta. Note increased staining of the VSMCs in the media (**inset** in **B**). Verhoeff-van Gieson (VVG) staining demonstrates medial and adventitial expansion in the Ren2 model (**D**) as compared to the SDC model (**C**). TUNEL staining depicts apoptosis in the adventitia and, to a lesser extent, in the endothelium and media in Ren2 rats (**F**) as compared to the SDC model (**E**). Note that elastin is autofluorescent (**E**, **F**). L = Lumen. Magnification ×40.

Light Microscopic Histological Preparation and Staining

The thoracic aorta was fixed in 3% paraformaldehyde, infiltrated and embedded in paraffin for light microscopic examination.

3-Nitrotyrosine Staining

For 3-nitrotyrosine (a known marker of tissue OS) staining, 4-µm aortic tissue sections were deparaffinized and rehydrated, and epitopes were retrieved in citrate buffer as previously described, imaged with a bright-field microscopy (Nikon 50i) and captured with a CoolSNAP *cf* camera [6].

TUNEL Staining

TUNEL staining was performed using the In Situ Cell Death Detection Kit according to the manufacturer's instructions, as previously described [7].

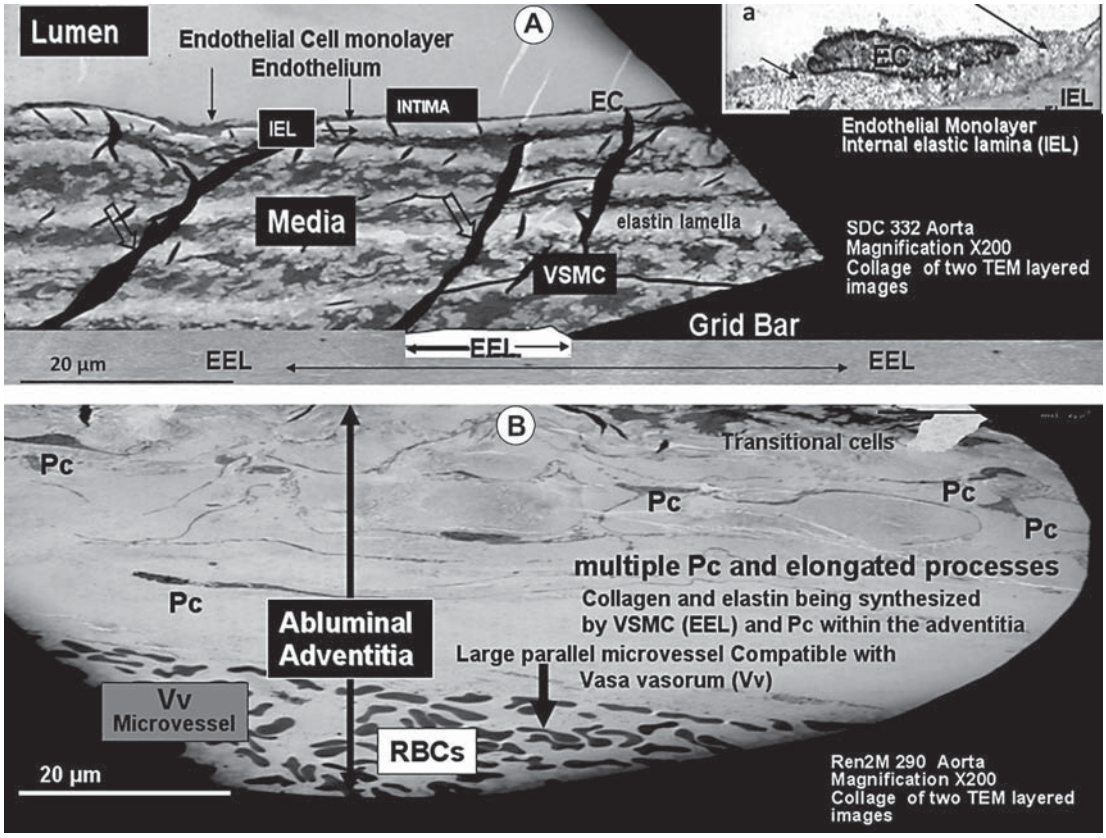

Fig. 3. This collage of two separate images merged together depicts the various layers of the thoracic aorta in the SDC model (**A**). The lumen, EC monolayer (arrows in **inset a**), IEL, media with its VSMCs (note the electron-dense elastin folds or 'garters', open arrows), external elastic lamina (EEL) and the disproportionately expanded abluminal adventitia layer from the Ren2 model emphasize the importance of its multiple pericytes (Pc) and long pericyte cytoplasmic processes (**B**). Note that at the bottom of this collage, a large periadventitial microvessel (vasa vasorum, Vv) is running parallel with the lumen containing multiple red blood cells (RBCs). Magnification ×200.

Statistics

Student's unpaired t test was used to determine statistical differences between the aortic parameters in the SDC and Ren2 models.

Results

Systolic Blood Pressure, Weight and Blood Glucose

Ren2 rats were more hypertensive, weighed less and had higher fasting blood glucose levels at the time of sacrifice (table 1).

Endothelium

The endothelium and its relation to the media and adventitial layers are depicted with light microscopy and a low-magnification TEM collage in figures 2 and 3, respectively. ECs of SDC were elongated and approximately 20 µm in length and tightly adherent to the IEL (fig. 3, 4); however, the Ren2 ECs were nearly all retracted and/or vertical, with a length of

Cardiorenal Med 2012;2:66–82
DOI: 10.1159/000335565
Published online: January 27, 2012

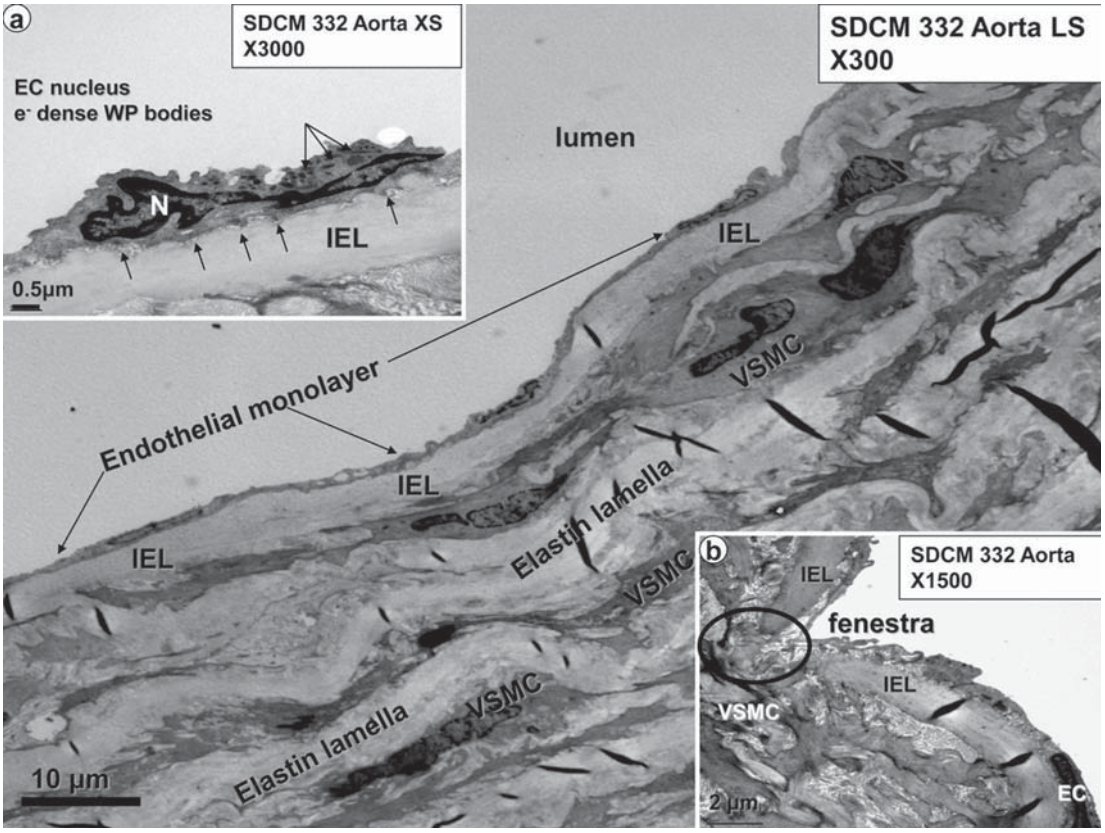

Fig. 4. Normal EC monolayer with the fenestrae, IEL and media in the SDC aorta. The normal EC measures approximately 20 μm in length, and the normal continuous EC monolayer (arrows) is tightly adherent to the underlying IEL, which separates the underlying media from the EC monolayer. The media is composed of alternating layers of VSMCs and elastin lamellae. In some longitudinal sections (LS), the VSMCs appear to be aligned nearly in parallel with the endothelium, whereas in other longitudinal sections and in almost all cross-sections (XS) the VSMCs appear to be arranged obliquely. Magnification ×300. **Inset a** portrays a higher magnification of an EC and its nucleus (N), with prominent cytoplasmic electron (e^-)-dense Weibel-Palade (WP) body organelles (luminal arrows). Note the endothelial basal adhesion plaques (hemidesmosome-like structures, abluminal arrows), which appear to be responsible for the tight adherence of the EC to the IEL. Magnification ×3,000. **Inset b** depicts a normal fenestra (myoendothelial junction) in the endothelial monolayer allowing direct contact and communication between the EC and VSMC. Magnification ×1,500.

only 8–12 μm (fig. 5). A large number of ECs were disrupted, leaving the IEL exposed in many areas, a process compatible with EC desquamation and erosion (fig. 5E, I). Even in ECs that remained adherent to the IEL, there was a previously undescribed phenomenon of nuclear 'terminal lifting' of the ECs (fig. 5C). Ren2 ECs demonstrated adjacent duplication and also a 'piggy-back' phenomenon at the edges of EC desquamation (fig. 5D, E, respectively). This novel finding may represent recent replication of the marginal EC or endothelial progenitor cell (EPC) homing attachments at the marginal EC, adjacent to regions of desquamation (fig. 6) [20, 21].

EC apoptosis (fig. 5G, H) was only observed in Ren2 models, and there was a central finding within the cytosol which we have termed cytosolic apoptotic loops (fig. 5H). We subsequently determined that these cytosolic apoptotic loops were a common finding, not only

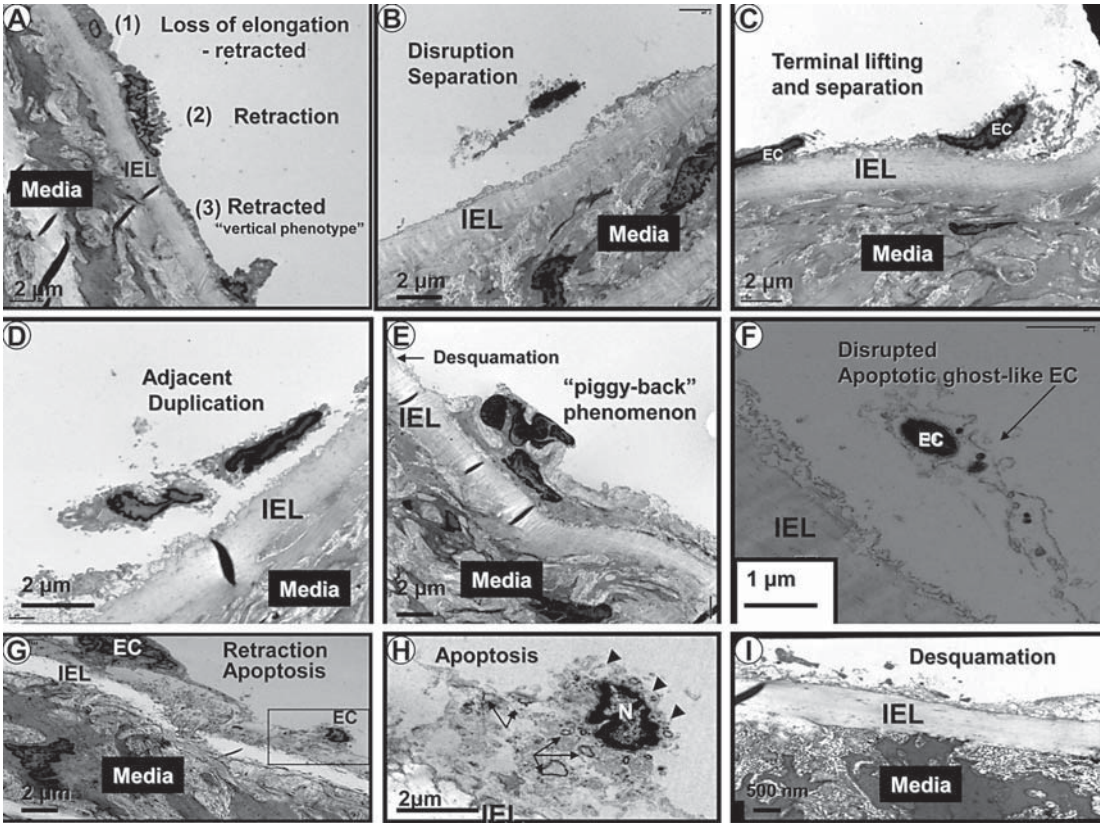

Fig. 5. Phenotypic changes of the Ren2 rat endothelium. This collection of EC phenotypic alterations demonstrates the various abnormal cellular remodeling of ECs in the Ren2 model. **A**, **B** and **C** represent EC retraction with vertical phenotype, disruption and the terminal nuclear lifting phenomenon with separation, respectively. **D**, **E** and **F** depict adjacent duplication, the 'piggy-back' phenomenon and a ghost-like apoptotic EC, respectively. **G**, **H** and **I** represent retraction, apoptosis and desquamation of the ECs, respectively. Note the presence of cytosolic apoptotic loops (arrows), the loss of plasma membrane integrity (arrowheads) and nuclear chromatin clumping (N) in **H**. Magnifications vary from image to image.

Table 1. Comparison of mean body weight, blood pressure and glucose of the Ren2 and SDC animal models

Parameter	Animal model		p value[a]
	Ren2	SDC	
Mean body weight, g	255 ± 4	274 ± 5	0.025
Initial blood pressure, mm Hg	144.2 ± 1.7	126.2 ± 3.7	0.005
Final blood pressure, mm Hg	160.9 ± 6.8	141.0 ± 0.5	0.027
Fasting blood glucose, mg/dl	162.0 ± 13.4	117.0 ± 7.2	0.025
	9.0 ± 0.7	6.5 ± 0.4	

[a] Unpaired Student's t test.

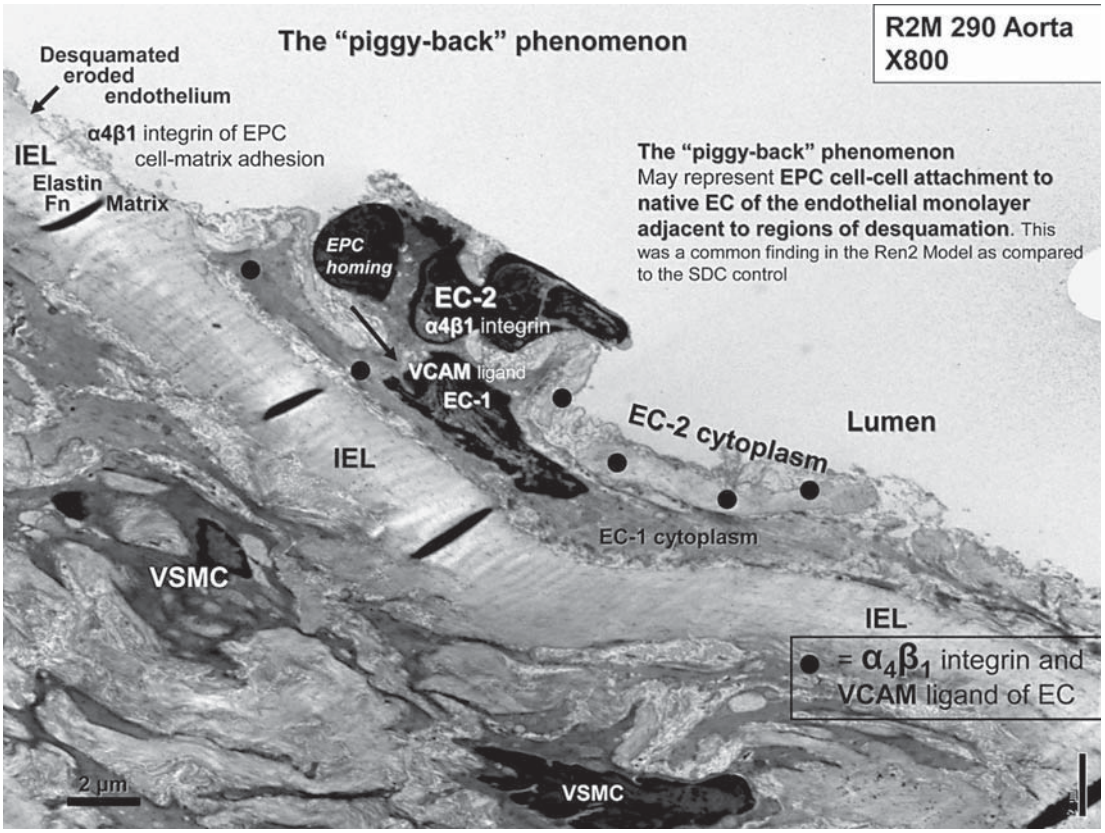

Fig. 6. The 'piggy-back' phenomenon. This image is a full plate of figure 5E to better understand this novel phenomenon. EC-1 is the native EC adjacent to an area of endothelial desquamation (arrow). EC-2 is noted to reside luminally in a 'piggy-back'-like fashion with multiple electron-dense adherens junctions of EC-2 to EC-1 (large black dots). These adherens junctions are accomplished via the β_1-integrin family binding to its ligand vascular cellular adhesion molecule (VCAM) ligands and subsequent vascular endothelial cadherins. Magnification ×800. Fn = Fibronectin.

the apoptotic ECs, but also the apoptotic VSMCs in the media and the pericytes in the adventitia. Additionally, ECs in the Ren2 model demonstrated a structural loss of plasma membrane integrity (fig. 5H).

Interestingly, there were EC secretory vesicles and caveolae present in the Ren2 rats, which were not present in the SDC vasculature (fig. 7). We suggest that in the Ren2 model, increased reactive oxygen species (ROS)/OS could upregulate caveolae and the endothelial nitric oxide synthase enzyme in order to offset the increased OS to the endothelium. In previous observational investigations [unpubl. data], an increased number of secretory granules and caveolae in the VSMC plasma membranes and ECs in pancreatic islets, pericytes and skeletal muscle tissue of the soleus and gastrocnemius skeletal muscles in the Ren2 model was observed as compared to the SDC model. Importantly, it is known that OS induces caveolin-1 gene transcription, which may help to understand our observations [22].

EC cytoplasmic organelles demonstrated a marked reduction in the number of Weibel-Palade bodies (WPBs), which were depleted 4–5-fold in the Ren2 endothelium as compared to the SDC model (fig. 4, 8). The hemostatic glycoprotein von Willebrand factor (vWF; a plasma marker of EC dysfunction, damage and activation) is synthesized in ECs and stored

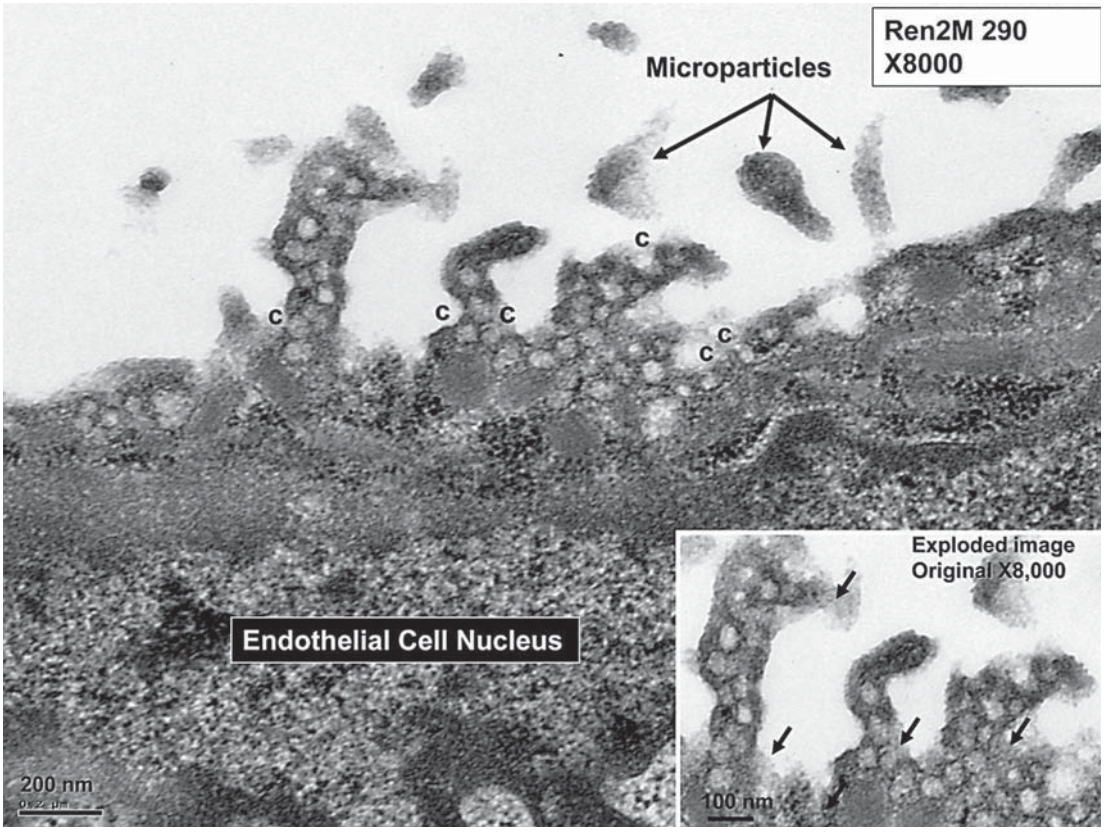

Fig. 7. This image depicts the presence of secretory granules and caveolae (c) in the EC projections in the Ren2 model. These could not be observed in the SDC model. Note the presence of variable electron-dense staining irregular particles in the lumen, which may represent microparticles. Magnification ×8,000. **Inset** depicts the secretory granules and caveolae in an exploded image. Note the residual glycocalyx, which is usually stripped away with fixation (arrows).

in WPB granules (lysosome-related storage and secretory organelles); therefore, it was not surprising that endothelial WPBs were depleted, since it is known that vWF serum levels are elevated in patients with HTN and atherosclerosis [23–26]. Depletion of WPBs in ECs from Ren2 rats could result in a prothrombotic milieu with impaired fibrinolysis, since tissue-type plasminogen activator is known to be co-localized along with vWf in these organelles [27, 28]. Additionally, WPBs are known to contain endothelin-1 (ET-1), and this depletion could increase the plasma level of active ET-1, possibly contributing to an increased contractile state together with the known activation of ET-1 by the increased local tissue levels of Ang II in Ren2 arterial tissue [27, 29].

Interestingly, there was a novel finding of marked attenuation of basal endothelial adhesion plaques in the Ren2 as compared to the SDC vasculature (fig. 9). These basal adhesion plaques were reminiscent of similar structures termed hemidesmosomes (cell-matrix attachments) that have been identified in laminitic ponies; therefore, the term hemidesmosome-like structures is appropriate. In laminitic ponies, the hemidesmosome structures act as adhesion plaques between the keratinocyte and the interstitial matrix (epithelial-matrix connections or adhesion plaques) and are reduced in number [30, 31]. In the SDC and Ren2 vasculature, these structures act as basal adhesion plaques between the EC and the elastin lamina matrix of the IEL [32].

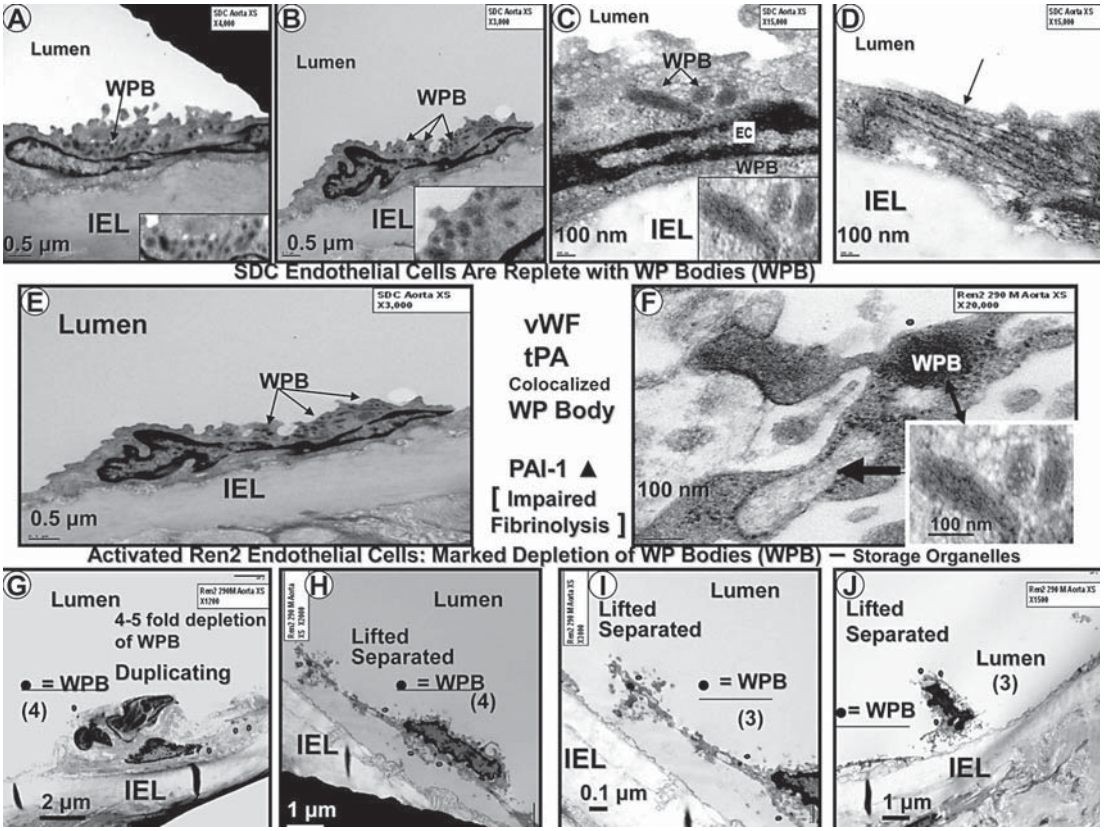

Fig. 8. This collection of TEM images demonstrates that EC cytoplasmic electron-dense WPBs (arrows) are present in the SDC model (**A–E**). Images in **C** and **F** (including **insets**) depict WPBs at higher magnification. WPBs can measure 100–200 nm in diameter and up to 1–5 μm in length (20-nm microtubules can be observed in the cross-section). The SDC model is replete with WPBs, whereas WPBs (dots) are markedly depleted in the Ren2 model (**G–J**). There is a 4–5-fold decrease in WPBs in the Ren2 model (20 WPBs in SDC vs. 3–4 WPBs in Ren2). **F** Immature and developing WPBs (arrow) were noted in the Ren2 model (mature WPB in the **inset**, double arrow). Magnifications vary from image to image.

Recently, it has been demonstrated that OS may activate nuclear transcription factors such as nuclear factor-kappa B (NF-κB) and subsequently activates downstream inflammatory cytokines such as tumor necrosis factor-alpha (TNF-α), resulting in vascular wall inflammation [7]. Also, OS is known to activate proteases such as matrix metalloproteinases (MMPs) including MMP-2 and MMP-9 [33, 34]. MMPs may then be responsible for the digestion of the media matrix and IEL and the hemidesmosome-like basal adhesion plaques as well as the cell-cell connections of ECs. Thus, we hypothesize that the loss of these hemidesmosome-like structures may be responsible for EC disruption, erosion, lifting, separation and desquamation and may contribute to EC apoptosis. Recent evidence has shown that EC and VSMC apoptosis is increased in the Ren2 model [32], making the loss of hemidesmosome-like structures extremely important. In addition to this loss, there may also be a loss of the cell-cell connections (vascular endothelial cadherins and β-catenins between adjacent ECs) [35–37].

Four basic types of EC cell-cell adherens junctions have been described, consisting of butt, overlap, mortise and complex junctions (fig. 10) [38]. These were found commonly in the SDC model, with the overlap junction being the most common. In contrast, EC cell-cell

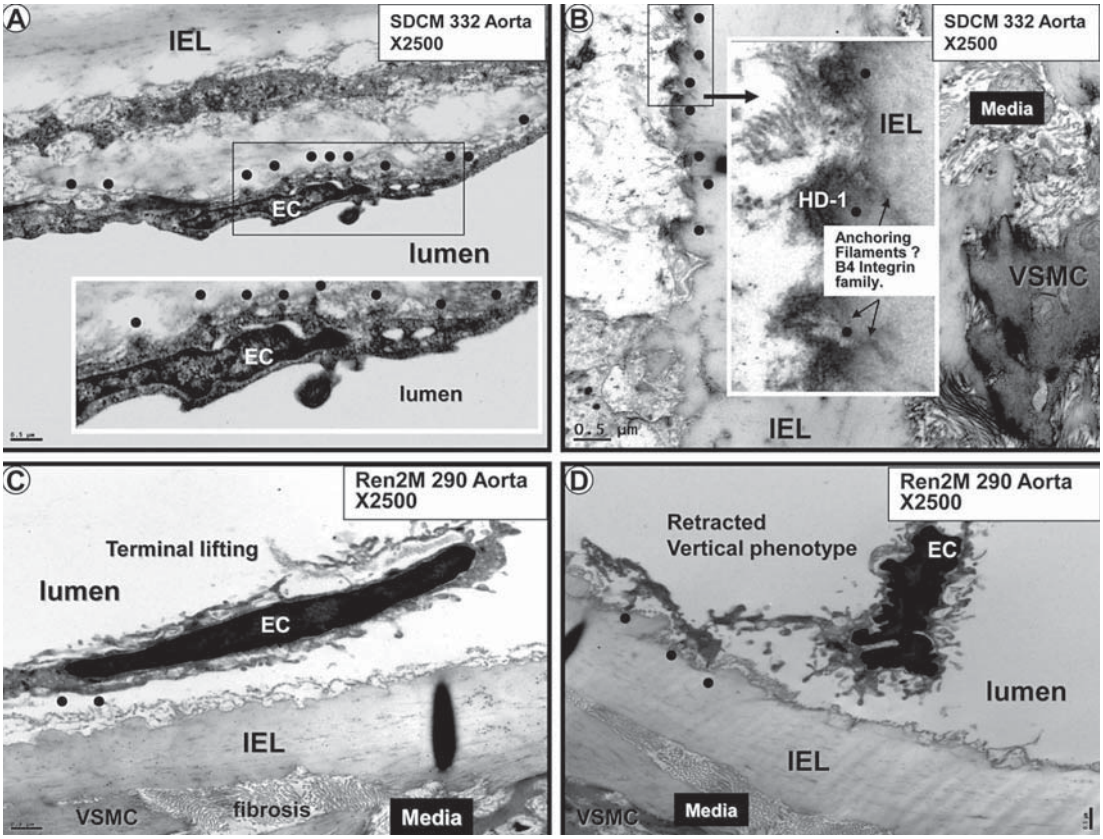

Fig. 9. A, **B** Endothelial basal adhesion plaques (hemidesmosome-like structures) in the SDC model (dots). **C**, **D** Loss of these hemidesmosome-like basal adhesion plaques (dots) in the Ren2 model. Magnification ×2,500. Bar = 0.5 μm. **Insets** in **A** and **B** depict the hemidesmosome-like structures at higher magnification (dots). Note the anchoring filaments of the hemidesmosome-like structures into the elastin of the IEL (dots) in the **inset** in **B**. The loss of these hemidesmosome-like structures results in the EC findings in figure 5. HD-1 = Hemidesmosome-1 protein.

and cell-matrix connections were lost in the Ren2 model, which, in addition to the loss of hemidesmosome-like structures, helps to explain our previous findings including EC desquamation and apoptosis (fig. 5). Importantly, we have recently been able to demonstrate ultrastructurally the attenuation and fragmentation of tight junctions between the capillary monolayer of ECs in a db/db obese type 2 diabetic mouse model [unpubl. data].

The above-described phenotypic changes in the Ren2 endothelium are indicative of structural endothelial activation and, therefore, it was not surprising that we found evidence of endothelial platelet adherence and activation (fig. 11) in the Ren2 model. Additionally, we observed what might be prothrombotic, proinflammatory and proendothelial dysfunction microparticles in the regions of EC activation and platelet adherence (fig. 7, 11). These microparticles are thought to be closely related to both EC and platelet activation and are strongly associated with endothelial dysfunction, OS, HTN, atherosclerosis and T2DM in the CRS [39–42]. Interestingly, we did not observe any leukocyte adherence to the endothelium or an accumulation of leukocytes within the newly created subendothelial space (neointima) in this model. Even though the Ren2 model is known to exhibit aortic vascular inflammation associated with NADPH oxidase activation and subsequent activation of NF-κB and downstream TNF-α [7], the neointima had just been created in the 9–10-week-old Ren2 rats

Cardiorenal Med 2012;2:66–82
DOI: 10.1159/000335565
Published online: January 27, 2012

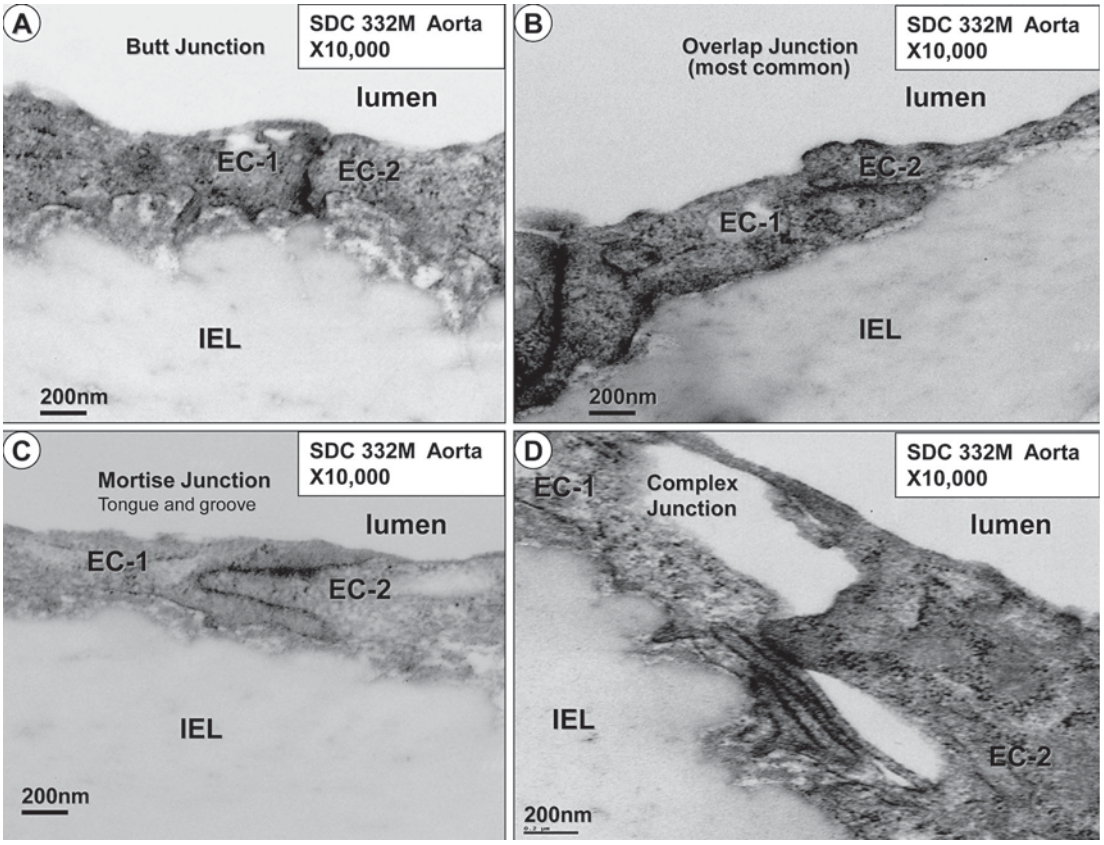

Fig. 10. The four most common endothelial monolayer cell-cell junctions. The abutment/butt junction (**A**), the overlap junction, which is the most common cell-cell junction among all cell-cell junctions found in the SDC and Ren2 models (**B**), the mortise or tongue and groove (peg-socket) cell-cell junction (**C**), and the complex cell-cell junction (**D**). When identified, the EC cell-cell junctions in the Ren2 model were usually of the overlap type; however, there was a marked impairment of EC cell-cell junctions in the Ren2 model. Magnification ×10,000.

and may possibly be too young to manifest intimal leukocyte adherence or neointimal inflammation. Another possibility is that the adherent leukocytes were removed during the fixation process.

Internal Elastic Lamina

The IEL is mostly a continuous structure with ECs tightly adherent on its luminal side and lined by a loose connective tissue matrix with VSMC cytoplasmic processes tending to its abluminal maintenance at variable distances (fig. 3–6, 12). The IEL matrix consists primarily of a homogenous, characteristic refractile-like elastin, and at higher magnification it is stippled with electron-dense proteoglycan core proteins (fig. 12A). This continuous supportive structure of the endothelium is normally interrupted by rounded ends of the IEL at sites referred to as fenestrae or myoendothelial junctions, and at these locations the ECs and VSMCs may undergo direct contact enabling them to experience direct cell-cell communication (fig. 12B). The number of fenestrae per unit length did not differ between the SDC and Ren2 models; however, more IEL- non-fenestra – IEL breaks (non-rounded with jagged ends of the IEL) did occur in the Ren2 model (fig. 12C). IEL duplica-

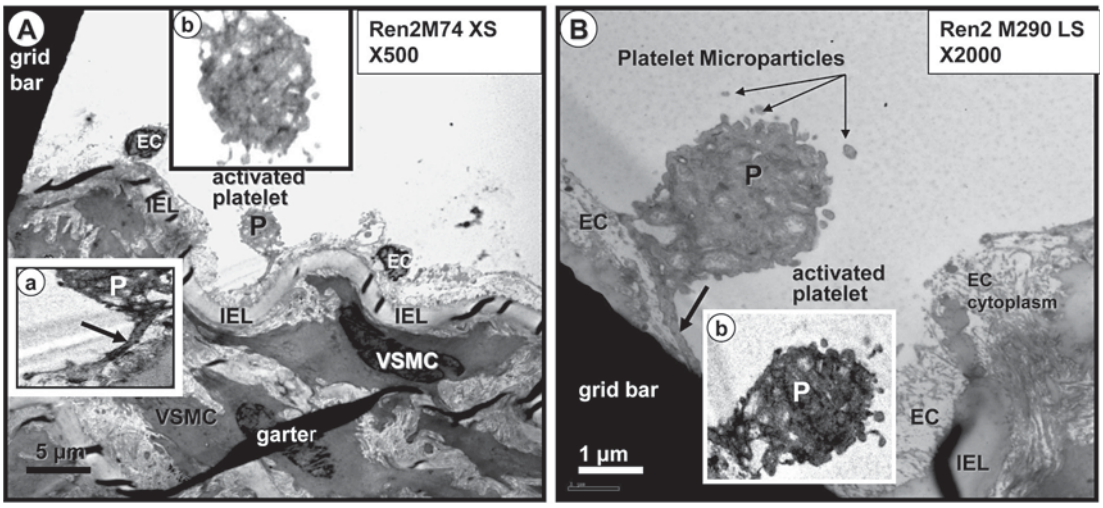

Fig. 11. Activated platelets adhering with pseudopods to an activated endothelium in the Ren2 model. **A** Adherent activated platelet (P). **Inset a** depicts the pseudopod attachment (arrow) to the underlying endothelium. **Inset b** demonstrates the marked depletion of coarse granules and the irregular pseudopod surface of the platelet. Magnification ×500. **B** Activated platelet (P) adhering to the endothelium in another Ren2 animal model. Note the depletion of coarse granules in this platelet and the platelet microparticles in the lumen adjacent to this activated platelet (arrows). **Inset b** highlights these changes. Magnification ×2,000.

tions were found only in the Ren2 model on luminal and abluminal surfaces where the IEL occasionally encased cytoplasmic VSMC structures (fig. 12D). Importantly, we were able to identify the breeching of the IEL by VSMCs and follow their migration to a newly created subendothelial space (neointima; depicted in greater detail in Part 2 of this two-part series).

Genesis of the Neointima in the Transgenic Ren2 Rat Aorta

Young rodents at 6 weeks of age do not have an existing subendothelial intimal space (intima) [43], making it possible to identify the genesis of the neointima in the Ren2 model due to increased local tissue Ang II and metabolic OS, IR, hyperinsulinemia with IGT and hypertensive stressors.

The Ren2 model demonstrated the genesis of a neointima at 9–10 weeks of age in some regions of the aorta, and this finding was not present in SDC aortas. The creation of a neointima is dependent on the activation of a more synthetic VSMC and its effects on the IEL with an eventual breeching of the IEL with subsequent migration into the subendothelial space (neointima) [44]. The genesis of the neointima will be discussed in greater detail in Part 2 of this two-part series.

Discussion

Commensurate with the functional changes of the endothelium resulting in aortic endothelial and vascular dysfunction [45], there are multiple ultrastructural vascular endothelial remodeling changes. The above-mentioned ultrastructural findings in the endothelium and the IEL as well as the genesis of a neointima allow the reader to have a better concept of

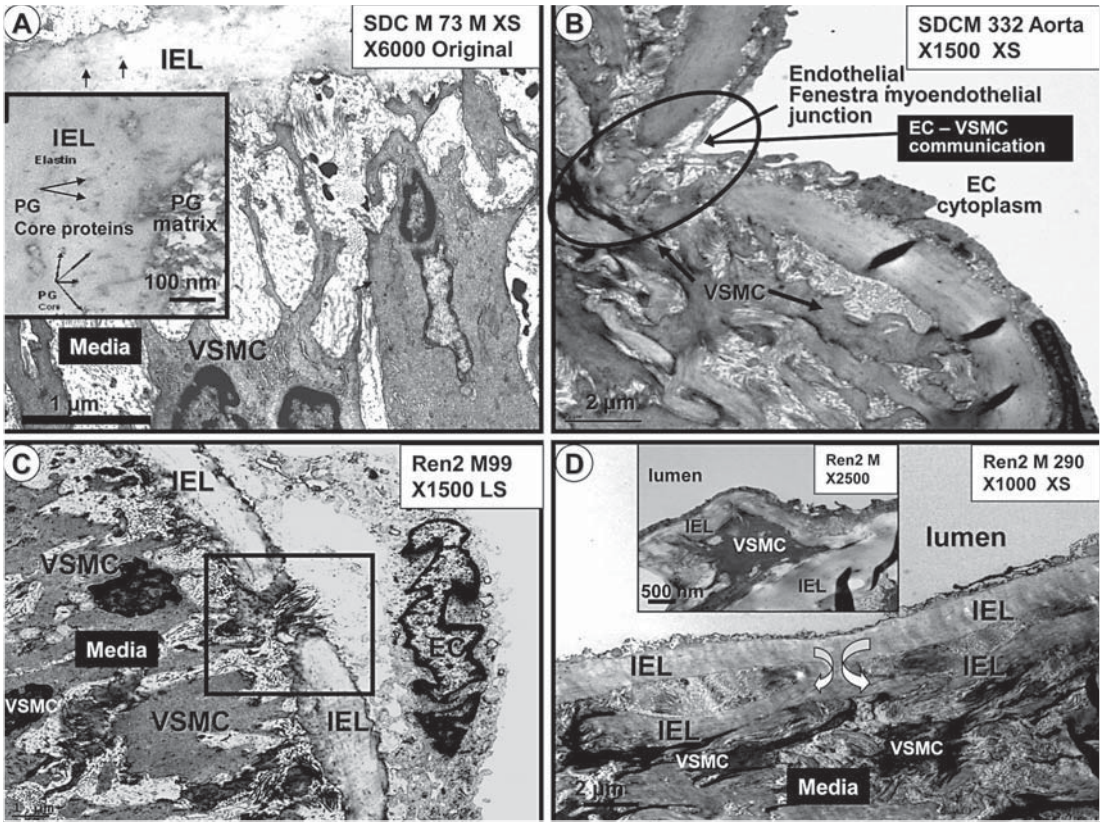

Fig. 12. IEL maintenance, fenestrations, breaks and duplications. **A** Depiction of the normal relation between the IEL and the media matrix in the SDC model. Note how the VSMC maintains and tends to the maintenance of the IEL. The IEL is homogeneous and somewhat refractile, with noticeable stippling due to proteoglycan (PG) core proteins (arrows) at higher magnification (**inset**). Magnification ×6,000. **B** Illustration of a typical endothelial fenestra (myoendothelial junction) found to be present in both the SDC and Ren2 models. Note the encircled area depicting the EC-VSMC contact and communication allowing crosstalk communication. Magnification ×1,500. **C** Image portraying a typical IEL break, demonstrating the jagged edges of the IEL as compared to the rounded smooth edges of the IEL of a normal fenestra depicted in **B**. These IEL breaks were increased and only found in the Ren2 model. Magnification ×1,500. **D** Demonstration of the duplication of the IEL found in the Ren2 model in the abluminal region of the IEL. Magnification ×1,000. Duplication is also present on the luminal side of the IEL and appears to encircle a VSMC (**inset**). Magnification ×2,500.

the earliest ultrastructural remodeling changes associated with HTN, accelerated atherosclerosis (atherosclerosis), IGT and renal disease in the CRS. Contemporaneous with the multiple metabolic stressor toxicities responsible for the excessive generation of ROS, OS and redox stress, one can now envision these exciting ultrastructural remodeling changes associated with the toxicity of HTN in this transgenic Ren2 rat model.

In summary, the endothelial changes in the hypertensive Ren2 rat model consisted of a decreased endothelial length with retraction, separation, terminal nuclear lifting, adjacent duplication, apoptosis and a suggestion of EPC attachment. Additionally, the endothelium demonstrated increased secretory vesicles, luminal caveolae, microparticles, depletion of WPBs, loss of cell-cell and basal adhesion hemidesmosome-like structures with loss of cell-matrix attachments and endothelial desquamation, platelet adhesion/activation and the gen-

esis of a subendothelial neointima. Since the genesis of the neointima is largely under the direction of the medial VSMCs and possibly the adventitia, these ultrastructural images will be depicted in Part 2 of this two-part series.

Acknowledgements

The authors would like to acknowledge the Electron Microscopic Core Center at the University of Missouri, Columbia, Mo., USA, for the preparation of animal tissue samples for viewing. We also acknowledge Brenda Hunter for her assistance in preparing the manuscript. This research was supported by NIH (R01 HL73101-01A1) and the Veterans Affairs Merit System (0018).

Disclosure Statement

The authors declare that they have no competing interests.

References

1 Blendea MC, Jacobs D, Stump CS, McFarlane SI, Ogrin C, Bahtyiar G, Stas S, Kumar P, Sha Q, Ferrario CM, Sowers JR: Abrogation of oxidative stress improves insulin sensitivity in the Ren-2 rat model of tissue angiotensin II overexpression. Am J Physiol Endocrinol Metab 2005;288:E353–E359.
2 Whaley-Connell AT, Chowdhury NA, Hayden MR, Stump CS, Habibi J, Wiedmeyer CE, Gallagher PE, Tallant EA, Cooper SA, Link CD, Ferrario C, Sowers JR: Oxidative stress and glomerular filtration barrier injury: role of the renin-angiotensin system in the Ren2 transgenic rat. Am J Physiol Renal Physiol 2006;291:F1308–F1314.
3 Hayden MR, Chowdhury NA, Cooper SA, Whaley-Connell A, Habibi J, Witte L, Wiedmeyer C, Manrique CM, Lastra G, Ferrario C, Stump C, Sowers JR: Proximal tubule microvilli remodeling and albuminuria in the Ren2 transgenic rat. Am J Physiol Renal Physiol 2007;292:F861–F867.
4 Habibi J, Whaley-Connell A, Qazi MA, Hayden MR, Cooper SA, Tramontano A, Thyfault J, Stump C, Ferrario C, Muniyappa R, Sowers JR: Rosuvastatin, a 3-hydroxy-3-methylglutaryl coenzyme a reductase inhibitor, decreases cardiac oxidative stress and remodeling in Ren2 transgenic rats. Endocrinology 2007;148:2181–2188.
5 Whaley-Connell A, Govindarajan G, Habibi J, Hayden MR, Cooper SA, Wei Y, Ma L, Qazi M, Link D, Karuparthi PR, Stump C, Ferrario C, Sowers JR: Angiotensin II-mediated oxidative stress promotes myocardial tissue remodeling in the transgenic (mRen2) 27 Ren2 rat. Am J Physiol Endocrinol Metab 2007;293:E355–E363.
6 Stas S, Whaley-Connell A, Habibi J, Appesh L, Hayden MR, Karuparthi PR, Qazi M, Morris EM, Cooper SA, Link CD, Stump C, Hay M, Ferrario C, Sowers JR: Mineralocorticoid receptor blockade attenuates chronic overexpression of the renin-angiotensin-aldosterone system stimulation of reduced nicotinamide adenine dinucleotide phosphate oxidase and cardiac remodeling. Endocrinology 2007;148:3773–3780.
7 Wei Y, Whaley-Connell AT, Chen K, Habibi J, Uptergrove GM, Clark SE, Stump CS, Ferrario CM, Sowers JR: NADPH oxidase contributes to vascular inflammation, insulin resistance, and remodeling in the transgenic (mRen2) rat. Hypertension 2007;50:384–391.
8 Hayden MR, Chowdhury N, Govindarajan G, Karuparthi PR, Habibi J, Sowers JR: Myocardial myocyte remodeling and fibrosis in the cardiometabolic syndrome. J Cardiometab Syndr 2006;1:326–333.
9 Hayden MR, Karuparthi PR, Habibi J, Wasekar C, Lastra G, Manrique C, Stas S, Sowers JR: Ultrastructural islet study of early fibrosis in the Ren2 rat model of hypertension. Emerging role of the islet pancreatic pericyte-stellate cell. JOP 2007;8:725–738.
10 Whaley-Connell A, Habibi J, Nistala R, Cooper SA, Karuparthi PR, Hayden MR, Rehmer N, DeMarco VG, Andresen BT, Wei Y, Ferrario C, Sowers JR: Attenuation of NADPH oxidase activation and glomerular filtration barrier remodeling with statin treatment. Hypertension 2008;51:474–480.
11 DeMarco VG, Habibi J, Whaley-Connell AT, Schneider RI, Heller RL, Bosanquet JP, Hayden MR, Delcour K, Cooper SA, Andresen BT, Sowers JR, Dellsperger KC: Oxidative stress contributes to pulmonary hypertension in the transgenic (mRen2)27 rat. Am J Physiol Heart Circ Physiol 2008;294:H2659–H2668.
12 Lastra G, Whaley-Connell A, Manrique C, Habibi J, Gutweiler AA, Appesh L, Hayden MR, Wei Y, Ferrario C, Sowers JR: Low-dose spironolactone reduces reactive oxygen species generation and improves insulin-stimulated glucose transport in skeletal muscle in the TG(mRen2)27 rat. Am J Physiol Endocrinol Metab 2008;295:E110–E116.

13 Whaley-Connell A, Habibi J, Cooper SA, Demarco VG, Hayden MR, Stump CS, Link D, Ferrario CM, Sowers JR: Effect of renin inhibition and AT1R blockade on myocardial remodeling in the transgenic Ren2 rat. Am J Physiol Endocrinol Metab 2008;295:E103–E109.
14 Wei Y, Clark SE, Morris EM, Thyfault JP, Uptergrove GM, Whaley-Connell AT, Ferrario CM, Sowers JR, Ibdah JA: Angiotensin II-induced non-alcoholic fatty liver disease is mediated by oxidative stress in transgenic TG(mRen2)-27(Ren2) rats. J Hepatol 2008;49:417–428.
15 Habibi J, Whaley-Connell A, Hayden MR, Demarco VG, Schneider R, Sowers SD, Karuparthi P, Ferrario CM, Sowers JR: Renin inhibition attenuates insulin resistance, oxidative stress, and pancreatic remodeling in the transgenic Ren2 rat. Endocrinology 2008;149:5643–5655.
16 Whaley-Connell A, Habibi J, Johnson M, Tilmon R, Rehmer N, Rehmer J, Wiedmeyer C, Ferrario CM, Sowers JR: Nebivolol reduces proteinuria and renal NADPH oxidase-generated reactive oxygen species in the transgenic Ren2 rat. Am J Nephrol 2009;30:354–360.
17 Hayden MR, Habibi J, Whaley-Connell A, Sowers D, Johnson MS, Tilmon R, Jain D, Ferrario C, Sowers JR: Nebivolol attenuates maladaptive proximal tubule remodeling in transgenic rats. Am J Nephrol 2010;31:262–272.
18 Glagov S: Hemodynamic risk factors: mechanical stress, mural architecture, media nutrition, and the vulnerability of arteries to atherosclerosis; in Wissler RW, Geer JC, Kaufman N (eds): The Pathology of Atherosclerosis. Baltimore, Williams and Wilkins, 1972, p 164.
19 Geer JC, Haust MD: Smooth muscle cells in atherosclerosis; in Pollak OJ, Simms HS, Kirk JE (eds): Monographs on Atherosclerosis. Basal, Karger, 1972, p 39.
20 Maeda M, Fukui A, Nakamura T, Inada Y, Tamai S, Haga S, Tatsumi-Nagano K, Yamamoto H, Ogata S, Iwata H, Ikada Y: Progenitor endothelial cells on vascular grafts: an ultrastructural study. J Biomed Mater Res 2000;51:55–60.
21 Peinado VI, Ramírez J, Roca J, Rodriguez-Roisin R, Barberà JA: Identification of vascular progenitor cells in pulmonary arteries of patients with chronic obstructive pulmonary disease. Am J Respir Cell Mol Biol 2006;34:257–263.
22 Dasari A, Bartholomew JN, Volonte D, Galbiati F: Oxidative stress induces premature senescence by stimulating caveolin-1 gene transcription through p38 mitogen-activated protein kinase/Sp1-mediated activation of two GC-rich promoter elements. Cancer Res 2006;66:10805–10814.
23 Metcalf DJ, Nightingale TD, Zenner HL, Lui-Roberts WW, Cutler DF: Formation and function of Weibel-Palade bodies. J Cell Sci 2008;121:19–27.
24 Zenner HL, Collinson LM, Michaux G, Cutler DF: High-pressure freezing provides insights into Weibel-Palade body biogenesis. J Cell Sci 2007;120:2117–2125.
25 Nadar S, Lip GY: The prothrombotic state in hypertension and the effects of antihypertensive treatment. Curr Pharm Des 2003;9:1715–1732.
26 Blann AD, McCollum CN: von Willebrand factor, endothelial cell damage and atherosclerosis. Eur J Vasc Surg 1994;8:10–15.
27 Emeis JJ, van den Eijnden-Schrauwen Y, van den Hoogen CM, de Priester W, Westmuckett A, Lupu F: An endothelial storage granule for tissue-type plasminogen activator. J Cell Biol 1997;139:245–256.
28 Rosnoblet C, Vischer UM, Gerard RD, Irminger JC, Halban PA, Kruithof EK: Storage of tissue-type plasminogen activator in Weibel-Palade bodies of human endothelial cells. Arterioscler Thromb Vasc Biol 1999;19:1796–1803.
29 Doi Y, Ozaka T, Fukushige H, Furukawa H, Yoshizuka M, Fujimoto S: Increase in number of Weibel-Palade bodies and endothelin-1 release from endothelial cells in the cadmium-treated rat thoracic aorta. Virchows Arch 1996;428:367–373.
30 Johnson PJ: The equine metabolic syndrome peripheral Cushing's syndrome. Vet Clin North Am Equine Pract 2002;18:271–393.
31 Johnson PJ, Kreeger JM, Keeler M, Ganjam VK, Messer NT: Serum markers of lamellar basement membrane degradation and lamellar histopathological changes in horses affected with laminitis. Equine Vet J 2000;32:462–468.
32 Wei Y, Whaley-Connell AT, Habibi J, Rehmer J, Rehmer N, Patel K, Hayden MR, DeMarco V, Ferrario CM, Ibdah JA, Sowers JR: Mineralocorticoid receptor antagonism attenuates vascular apoptosis and injury via rescuing protein kinase B activation. Hypertension 2009;53:158–165.
33 Mujumdar VS, Aru GM, Tyagi SC: Induction of oxidative stress by homocyst(e)ine impairs endothelial function. J Cell Biochem 2001;82:491–500.
34 Tyagi SC, Hayden MR: Role of nitric oxide in matrix remodeling in diabetes and heart failure. Heart Fail Rev 2003;8:23–28.
35 Herren B, Levkau B, Raines EW, Ross R: Cleavage of beta-catenin and plakoglobin and shedding of VE-cadherin during endothelial apoptosis: evidence for a role for caspases and metalloproteinases. Mol Biol Cell 1998;9:1589–1601.
36 Lampugnani MG, Corada M, Caveda L, Breviario F, Ayalon O, Geiger B, Dejana E: The molecular organization of endothelial cell to cell junctions: differential association of plakoglobin, beta-catenin, and alpha-catenin with vascular endothelial cadherin (VE-cadherin). J Cell Biol 1995;129:203–217.
37 Corada M, Mariotti M, Thurston G, Smith K, Kunkel R, Brockhaus M, Lampugnani MG, Martin-Padura I, Stoppacciaro A, Ruco L, McDonald DM, Ward PA, Dejana E: Vascular endothelial-cadherin is an important determinant of microvascular integrity in vivo. Proc Natl Acad Sci USA 1999;96:9815–9820.
38 Schwartz SM, Stemerman MB, Benditt EP: The aortic intima. II. Repair of the aortic lining after mechanical denudation. Am J Pathol 1975;81:15–42.

39 Lip GY: Hypertension, platelets, and the endothelium: the 'thrombotic paradox' of hypertension (or 'Birmingham paradox') revisited. Hypertension 2003;41:199–200.
40 Preston RA, Jy W, Jimenez JJ, Mauro LM, Horstman LL, Valle M, Aime G, Ahn YS: Effects of severe hypertension on endothelial and platelet microparticles. Hypertension 2003;41:211–217.
41 Boulanger M, Amabile N, Tedgui A: Circulating microparticles: a potential prognostic marker for atherosclerotic vascular disease. Hypertension 2006;48:180–186.
42 Leroyer AS, Tedgui A, Boulanger CM: Microparticles and type 2 diabetes. Diabetes Metab 2008;34(suppl 1):S27–S32.
43 Guyton JR, Lindsay KL, Dao DT: Comparison of aortic intima and inner media in young adult versus aging rats. Stereology in a polarized system. Am J Pathol 1983;111:234–246.
44 Ross R: The pathogenesis of atherosclerosis: a perspective for the 1990s. Nature 1993;362:801–809.
45 Arnet UA, Novosel D, Barton M, Noll G, Ganten D Luscher TF: Endothelial dysfunction in the aorta of transgenic rats harboring the mouse Ren-2 gene. Endothelium 1999;6:175–184.